

Article

Alaskan Permafrost Groundwater Storage Changes Derived from GRACE and Ground Measurements

Reginald R. Muskett * and Vladimir E. Romanovsky

Geophysical Institute, University of Alaska Fairbanks, P.O. Box 757230, 903 Koyukuk Drive, Fairbanks, AK 99775, USA; E-Mail: veromanovsky@alaska.edu

* Author to whom correspondence should be addressed; E-Mail: reginald.muskett@gmail.com; Tel.: +1-907-474-1925; Fax: +1-907-474-7290.

Received: 1 December 2010; in revised form: 20 February 2011 / Accepted: 21 February 2011 / Published: 22 February 2011

Abstract: The Arctic is in transition from climate-driven thawing of permafrost. We investigate satellite-derived water equivalent mass changes, snow water equivalent with *in situ* measurements of runoff and ground-survey derived geoid models from 1999 through 2009. The Alaskan Arctic coastal plain groundwater storage (including wetland bog, thaw pond and lake) is increasing by $1.15 \pm 0.65 \text{ km}^3/\text{a}$ (area-average $1.10 \pm 0.62 \text{ cm/a}$), and Yukon River watershed groundwater storage is decreasing by $7.44 \pm 3.76 \text{ km}^3/\text{a}$ (area-average $0.79 \pm 0.40 \text{ cm/a}$). Geoid changes show increases within the Arctic coastal region and decreases within the Yukon River watershed. We hypothesize these changes are linked to the development of new predominately closed- and possibly open-talik in the continuous permafrost zone under large thaw lakes with increases of lakes and new predominately open-talik and reduction of permafrost extent in the discontinuous and sporadic zones with decreases of thaw lakes.

Keywords: permafrost; Talik; climate change; groundwater changes; Alaska; GRACE

1. Introduction

Arctic geomorphology, ecosystems, surface and groundwater are undergoing changes from permafrost thawing as a response to changing climate [1]. Permafrost is the largest component of the cryosphere [2]. Degradation of ice-rich permafrost can lead to significant surface subsidence affecting

changes in ecosystem, landscape, and where human habitats are established, significant infrastructure damage if not adequately considered in design [3,4]. The processes of freezing and thawing of the active layer, growth and degradation of permafrost affects the land surface energy and moisture fluxes (balances) which in turn impact biogeochemical cycles, climate and hydrologic systems [3,5,6].

Hydrologic processes in Arctic watersheds are controlled by permafrost distribution, talik configuration and the thickness of the active layer [3,4,7]. Talik is unfrozen earth material formed by hydrothermal and thermal processes near and beneath the ground surface and within permafrost [8]. Wildfires in boreal forest and tundra can alter the ground thermal regime resulting in warming and thawing of permafrost, active layer deepening and leading to talik formation [9]. Closed and open talik can be laterally extensive within permafrost. It can occur beneath lakes and rivers crossing the continuous and discontinuous permafrost zones. Open talik within permafrost connects the ground surface to the unfrozen material beneath permafrost allowing for recruitment of surface water into groundwater storage and loss of groundwater storage into surface water. In wintertime, base flow of rivers in permafrost watersheds, while reduced relative to non-permafrost watersheds, is maintained by water leaving groundwater storage [5,10,11]. Liquid water residing within cold and warm permafrost affects the ground thermal state [12]. The effect is largest near the ground surface and active layer after freeze-up, with stronger thermal gradients at the ground surface and increased heat flux.

Diverse observations across the high-latitude northern hemisphere indicate permafrost temperatures down to about 20 meters depth have increased over the twentieth century [13-15]. These are correlated to surface air temperature changes on decadal time scales [6]. Permafrost temperatures in northern Siberia, northern Alaska and northwest Canada have shown the largest magnitude of increases of a few degrees Celsius. Increased surface air temperatures from climate warming over the same period often cannot fully account for increased permafrost temperatures, suggesting that variability in snow cover may be a contributing factor [16]. Satellite data suggest that the total area of thermokarst lakes increased up to 12% in the northern continuous permafrost zone in western Siberia through processes of permafrost degradation, and the number of all lakes increased by 4% over the last 30 years [17]. However, in the southern discontinuous, sporadic and isolated permafrost zones the lake area showed losses up to 13% and the number of lakes decreased up to 9%. This suggests a linkage of permafrost and lake disappearance with extensive talik development.

Our investigation focuses on the trends of water equivalent mass changes within the Alaskan Arctic coastal plain and foothills, and the Yukon River watershed in Alaska and Yukon Territory using satellite geodesy and *in situ* measured runoff (Figure 1). This is one of our ongoing investigations of GRACE-derived terrestrial water storage changes on the Arctic watersheds of the northern hemisphere (Figure 2) [18]. We examine the regionalized trends and variations in water equivalent mass changes derived from geoid models and from the Gravity Recovery And Climate Experiment (GRACE) relative to the character and distribution of permafrost in these regions. We use data on snow water equivalent derived from the Special Scanning Microwave/Imager (SSM/I) sensor to provide us with wintertime water mass changes. Runoff data come from river gauge stations (ArcticRIMS, Arctic Freshwater Systems, and the US Geological Survey) are used for monthly water mass changes.

Figure 1. ESA Altimetry Corrected Elevation version-2 Global Digital Elevation Model shaded relief showing Alaska, USA, and western Canada. The Yukon River watershed (YRW) extent, Arctic Foothills (AF) and Arctic Coastal Plain (ACP) are delineated (white). Permafrost zone extents of the Isolated-Sporadic (yellow), Discontinuous (brown), and Continuous (red) are based on Jorgenson *et al.* (2008).

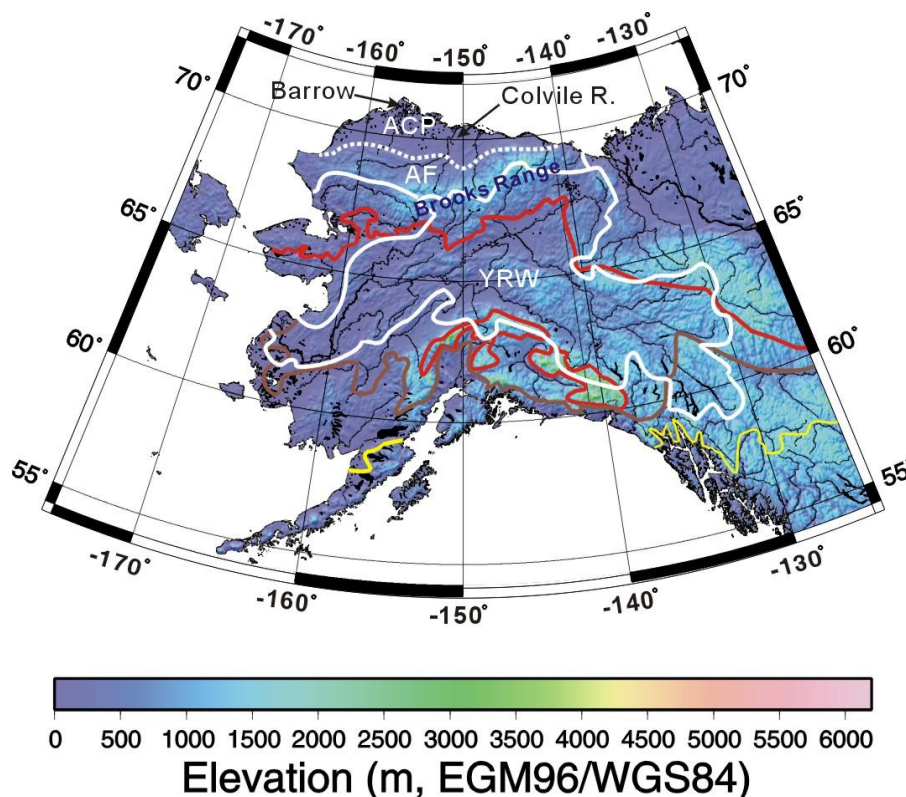


Figure 2. GRACE water equivalent mass changes on the northern hemisphere (top) and Alaska-western Canada (bottom) during May 2008 (left) and September 2008 (right) are shown. The Yukon River watershed and the Arctic foothills-coastal plain are delineated. Other important permafrost watersheds in Eurasia (Lena, Yenisei and Ob’) and North America (Mackenzie) are shown [18]. The seasonal maximum and seasonal minimum water equivalent mass change occur in May and September, respectively.

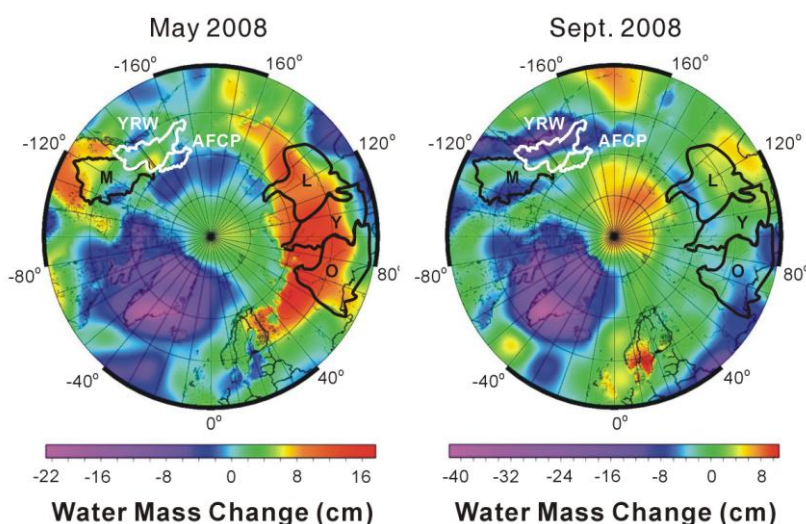
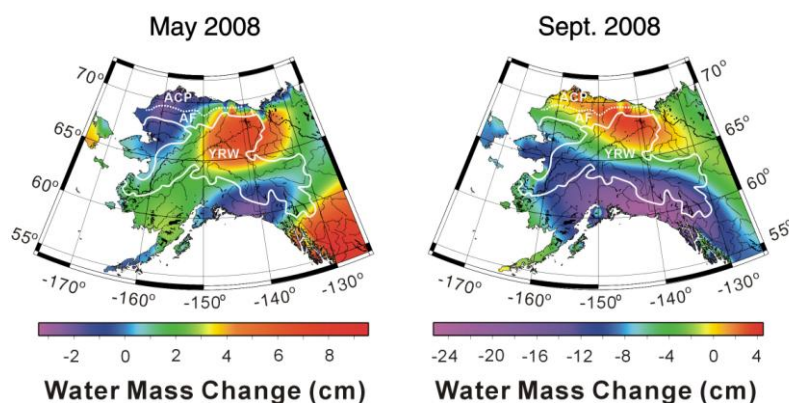


Figure 2. Cont.



2. Regions of Interest for Permafrost Zone Water Mass Changes

The Alaskan Arctic coastal plain (Figure 1), an area of about 104,000 km², is noted for its near-flat topography of tundra-wetland ecosystems, numerous thaw lakes and thick, up to 600 m, permafrost in the continuous permafrost zone [19-21]. The Barrow Peninsula area is noted for its large and numerous thaw lakes with their distinctive elliptic-shape and orientation [22]. Patterned ground formed by seasonal freeze-thaw and ice-wedge growing processes are common throughout this region. The Arctic coastal foothills (Figure 1), an area of about 120,000 km² forms a low-relief rolling topography incised by numerous rivers. Some of the rivers crossing the central and eastern foothills have a glacial melt-water component in their summer-time discharge [23].

The Brooks Range forms the meteorological-climatologic boundary of the Arctic in Alaska [24]. Permafrost in this area is much thinner and may be less than 200 m in many locations [19]. Precipitation within the Alaskan Arctic coastal plain and foothills is on the order of 100 mm in summer. Over the twentieth century, the number of days below freezing has been on the order of 300. Winter snowfall has been on the order of 80 cm with snow depths on the order of 20 to 50 cm [25,26]. Annual air temperatures recorded at Barrow, Alaska, from 1949 through 2005 had increases on the order of 2 °C [24]. Seasonal air temperature had increases of 0.8 °C in autumn and 3.2 °C in winter. Annual precipitation had decreases on the order of 2 cm. Seasonal precipitation had decreases of 1.3 cm in winter with summer unchanged, over the same period. Interannual and decadal variability affects the long-term trends, causing short interim periods of rapid changes or periods of neither increasing nor decreasing trend. On a monthly basis, peak precipitation of about 2 cm occurs in August.

The Yukon watershed (Figure 1) covers an area of 853,300 km² [27]. It is noted for its lowland wetland boreal ecosystems and high-elevation Alpine tundra, and is underlain by the discontinuous and sporadic permafrost zones [21]. Permafrost, where present, thickness ranges from about 15 m and less in the lowland western portions to about 180 m in the northeastern portions [28]. Headwaters of the tributaries of the Yukon River originate in the high-elevations of the Alaska and Brooks Ranges, in Alaska, and the Coast Mountains in Yukon Territory, Canada. Many are fed by summertime glacial-melt and wintertime base flow from groundwater [23,27]. It discharges its freshwater, suspended sediment, and dissolved carbon load at the Yukon Delta on the shores of the Bering Sea [29,30]. Freshwater from the Yukon watershed flowing northward through the Bering Strait contributes to the freshwater budget of the Arctic Ocean [31].

Precipitation in the Yukon River watershed, in Alaska, is relatively light and irregular on an annual basis and summer being peak season [24]. Annual temperatures recorded at Fairbanks, Alaska, from 1949 through 2005 had increases on the order of 2 °C. Autumn temperatures had decreases of 0.5 °C, and winter had increases of 4.6 °C. Annual precipitation had increases on the order of 0.3 cm. Summer precipitation had decreases of 0.5 cm and winter had decreases of 1 cm over the same period. Interannual and decadal variability strongly affects the long-term trends with the largest increase in precipitation occurred during 1976/77. Before and after this shift, neither increasing nor decreasing trends are apparent. On a monthly basis, peak precipitation of about 3 cm occurs in July.

3. Data

3.1. NOAA National Geodetic Service Geoid Models

Since the early 1990s the NOAA National Geodetic Survey (NGS) have been working on developments of high-spatial resolution and high-accuracy geoid models as part of the US national mapping and geodetic control network modernization programs [32,33]. The efforts centered on producing geoid models using ground-based gravimetric geoid observations (within the US and territorial coastal waters) at the US High-Accuracy Reference Network sites with Global Position System station coordinate determinations with long-wavelength undulations from the Earth Gravity Model 1996 (EGM96) a 360-degree and -order 15-arc-minute model and realization with respect to the International Terrestrial Reference Frame (ITRF) in the non-tide geodetic reference convention [34]. The first model was GEOID 1996 (GEOID96) a 2-arc-minute grid. It was followed in 1999 by the 1-arc-minute model GEOID99. Models GEOID03 and GEOID06 followed this. The latest efforts have produced GEOID09 that incorporates EGM2008, a 2,159-degree and -order 1-arc-minute model. GEOID99 and GEOID09 are the principle geoid models we use. The geoid models are relative to the WGS84 reference ellipsoid non-tide system in the convention of the International Terrestrial Reference Frame 2005.

3.2. Adjustment from GPS Stations

Adjustment for post-glacial and neotectonic (isostatic) changes were implemented by using Global Positioning System station position velocities at sites operated by US and Canada agencies for the International Terrestrial Reference System and the Earthscope Plate Boundary Observatory (<http://pboweb.unavco.org>) in Alaska and western Canada [35]. Realization of the station vertical velocities was in respect to the International Terrestrial Reference Frame 2005. GPS vertical velocities at fifty stations were fitted with a biharmonic spline surface satisfying minimum curvature using the technique of Sandwell [36]. This technique has become widely available and is incorporated in MatLab and Generic Mapping Tools programming packages [37].

3.3. GRACE

The joint US-German (NASA-GFZ) Gravity Recovery and Climate Experiment (GRACE) provide nominal-monthly near-surface water equivalent mass changes [38,39]. The tandem satellites measure variations in gravity/mass indirectly through changes of the inter-satellite range and range rate from an

initial orbit altitude of 485 km, in a controlled free-fall (down to about 200 km) non-repeating ground track mode. The mass changes are coupled to high accuracy onboard GPS and star-tracking instruments to reference them to the International Terrestrial Reference Frame 2005.

In our study we used the Release-04 (R4) Level-3 grids provided by the GRACE Science Team centers. The global grids are 1-arc-degree water equivalent mass change complete to degree and order 40 (ftp://podaac.jpl.nasa.gov/pub/tellus/monthly_mass_grids/). The GRACE solution to the gravity potential formulated as an equivalent water mass change (length scale) is given by

$$\Delta h(\phi, \lambda, t) = \frac{a_e \rho_e}{3\rho_w} \sum_{l=0}^{40} \sum_{m=0}^l \frac{(2l+1)}{1+k_l} W_l P_{lm} \sin(\phi) [\Delta C_{lm}(t) \cos(m\lambda) + \Delta S_{lm}(t) \sin(m\lambda)] \quad (1)$$

$$W_l = \exp\left[\frac{(lr/a_e)^2}{4 \ln(2)}\right]$$

P_{lm} : Normalized Legendre polynomials,

$\Delta C_{lm}(t)$, and $\Delta S_{lm}(t)$: Normalized time-varying Stokes spherical harmonic geopotential coefficients,

a_e : Earth mean radius,

r : spatial radius,

k_l : Love numbers,

ρ_e : Earth mean density,

ρ_w : water density,

t : time, and ϕ , λ are latitude and longitude [38].

Beyond degree (order) 40 to 70, the inherent noise level in the mass change signal becomes significant [40]. Processing includes downward propagation and adjustments to remove the time-variable mass change effects from tides and atmosphere and mean variation (GRACE geoid model). A normalized Gaussian smoother filter removes striping artifacts produced by the orbit non-crossing and control-descent geometry [38-40]. Differences in processing (de-aliasing) and error sources and products are attributable to differences in assumed zero-degree and order Stokes harmonics, tide (liquid and solid) models and the modeled atmosphere mass change removal, respectively in decreasing order of magnitude [41,42].

The GRACE R4 Level-3 (300 km smoothing kernel) land and ocean monthly grids from August 2002 through December 2008 were combined to give global coverage. Glacial isostatic adjustment (GIA), solid mass flow within the Earth's mantle following the decay of the Pleistocene Laurentide and Cordilleran ice sheets in North America and Euro-Scandinavia is an adjustment we applied to the GRACE grids. We implemented this adjustment using a GIA grid that uses the ICE-5G (VM2) provided by the GRACE science team [43,44].

3.4. Snow Water Equivalent

Global snow water equivalent estimates were derived from the NOAA Defense Meteorological Satellite Program by the Special Scanning Microwave/Imager (SSM/I) sensor [45]. We use data provided by the National Snow and Ice Data Center (NSIDC, <http://nsidc.org/data/nsidc-0271.html>). Snow water equivalent estimates in units of millimeters were derived using the horizontally polarized

difference algorithm for the 19 and 37 GHz channels from daily orbit swath acquisitions [46]. Missing retrievals due to swath coverage gaps are interpolated from neighboring swaths. Nominal spatial resolution is about 69 and 43 km² of the principal retrieval channels. Retrievals are obtained from a field of view of up to 625 km². Retrievals contain a mixed signal from terrain and vegetation types. Under-estimations can occur on extreme elevation mountains of complex geometry, along marine-coastlines where signals from ocean bodies are partly convolved, and the beginning and ending of the snow season when snow depths are thin and moist [47,48]. Noise from transitory atmosphere conditions is removed using a five-day filter. Monthly composite climatology is processed from daily passed-retrievals by averaging. Processed data are gridded in the equal-area scalable Earth (EASE) projection system at 25-km grid intervals.

3.5. Watershed Runoff

Measurements of surface water discharge (runoff) at gauge stations in the watersheds are provided by ArcticRIMS (<http://rims.unh.edu>), Arctic Freshwater Systems (<http://nhg.unbc.ca/ipy/>), in association with the US Geological Survey (<http://waterdata.usgs.gov/ak/nwis>). Over the 1950–2000 period of the data bases (Arctic Eurasian rivers) the error level as a percentage of total annual discharge is about 1.5 to 3.5% [49]. On our shorter time period and fewer rivers stream-gauge measurements typically have an uncertainty in the 10% to 20% range [50]. Monthly discharge from 2002 through 2008 at Pilot Station near the mouth of the Yukon watershed, gauge stations on the Colville River at Umiat, Kuparuk River and Sagavanirktok River near Deadhorse and Prudhoe Bay were used. Colville, Kuparuk and Sagavanirktok discharges were summed to give a single monthly time series for the Arctic coastal plain and foothills. We then derived annual time series of runoff by summing the monthly runoff from August through July periods. August through July was chosen as this period coincided with the GRACE time series instead of the typical water-year calendar convention.

4. Method

We derive area longitude-latitude extents of the Arctic coastal plain, foothills and the Yukon River watershed. The area-extents are used to extract GRACE and SSM/I data to compose regionalized time series of the mean, standard deviation and standard error. We compare these with monthly runoff for timing of winter snow water mass loading and spring surface water unloading. We then derive optimal least squares trends for comparison of trend gradients.

4.1. Theory of Water Mass Changes

On a global basis GRACE measures variations of the gravity field corresponding to the total change of mass from multiple sources [51,52]. On terrestrial non-glacier regions the mass changes will include those from snow, soil and vegetation moisture, lake storage, ground-ice, runoff and groundwater storage. Previously we found that the regionalized gradients of soil and vegetation moisture did not make significant contributions to regionalized total water equivalent storage change on the Arctic permafrost watersheds [18].

The regionalized gradient of total water equivalent storage change from GRACE (ΔT_{GRACE}) is the sum of the gradients of sub-surface (groundwater storage change, ΔG) and surface water storage change (runoff, ΔR)

$$\Delta T_{GRACE} \approx \Delta G + \Delta R \quad (2)$$

In this algebra ΔG is the unknown. Reducing ΔT_{GRACE} by ΔR yields the regionalized gradient of groundwater storage change

$$\Delta G \approx \Delta T_{GRACE} - \Delta R \quad (3)$$

In our formalism the regionalized gradient of groundwater storage change includes second-order regionalized gradients of storage changes in lakes, active layers, hyporheic zones and ground-ice bodies. Therefore, Equation (3) forms our theory of measurement. We estimate uncertainties from the trends and formal errors through the error propagation equation [53]. In this respect the estimate of the uncertainty of groundwater storage change gradient is the root sum of the squares of the uncertainties of GRACE total water storage change gradient and the area-average runoff gradient.

In our formulation there exist the Hilbert Space Ω , where the functions T , G and R exist and have sub-spaces τ , γ , and ρ [54]. T , G and R and the sub-spaces are linearly independent. Equation (3) formalizes a reduction of ΔT by ΔR in Ω to derive ΔG . This is not the so-called hydrologic balance. In applications, our formalism is the same philosophy as employed in Geopotential Theory, also in Harmonic Analysis, to reduce the total potential (field) by the strongest component potentials (fields) to derive an unknown component potential (field) [55]. As such the derived potential (field) ΔG may contain potentials (fields) of third and lesser order.

We use geoid models GEOID99 and GEOID09 to compute a geoid-difference model. This model is adjusted by using a trend surface derived from GPS vertical rates to remove isostatic effects in the period from 1999 through 2009. In theory, on short time scales and with removal of atmosphere, tide and solid-Earth isostatic effects, geoid changes should reflect changes of surface and groundwater storage and flows. We note that the models GEOID99 and GEOID09 are not completely independent. Differencing them will remove common features and present a net change of the Earth's geoid in Alaska and western Canada from 1999 through 2009.

5. Results

5.1. Regionalized Time Series and Gradients of Water Equivalent Mass Changes

Regionalized time series of GRACE, SSM/I, and *in situ* measured runoff show monthly water equivalent mass variations within Alaskan Arctic coastal plain, foothills and the Yukon River watershed regions (Figure 3). Gradient and uncertainties of water equivalent mass change in units of thickness (cm) water equivalent mass change are given in Table 1 and graphically in Figure 4.

The seasonal cycle of GRACE-derived water equivalent mass changes are evident within the Yukon watershed. The seasonal cycle of water equivalent mass changes within the Arctic foothills has a much smaller range, relative to the Yukon watershed. The seasonal cycle of water equivalent mass changes within the Arctic coastal plain had a much smaller range, relative to the Arctic foothills. On the Yukon watershed and Arctic foothills GRACE-derived minima occur in September–October and maxima

occur in April–May. SSM/I-derived snow water equivalent maxima occur in February–March with minima in June–September. Runoff-derived maxima occur in June with minima in December–April.

Figure 3. Regionalized time series of water mass changes and trends. Symbols refer to GRACE (orange filled squares), SSM/I SWE (light blue filled diamonds) and monthly runoff MR (blue bars) with annual runoff (August through July, light blue filled circles). T-bars denote regionalized standard deviations.

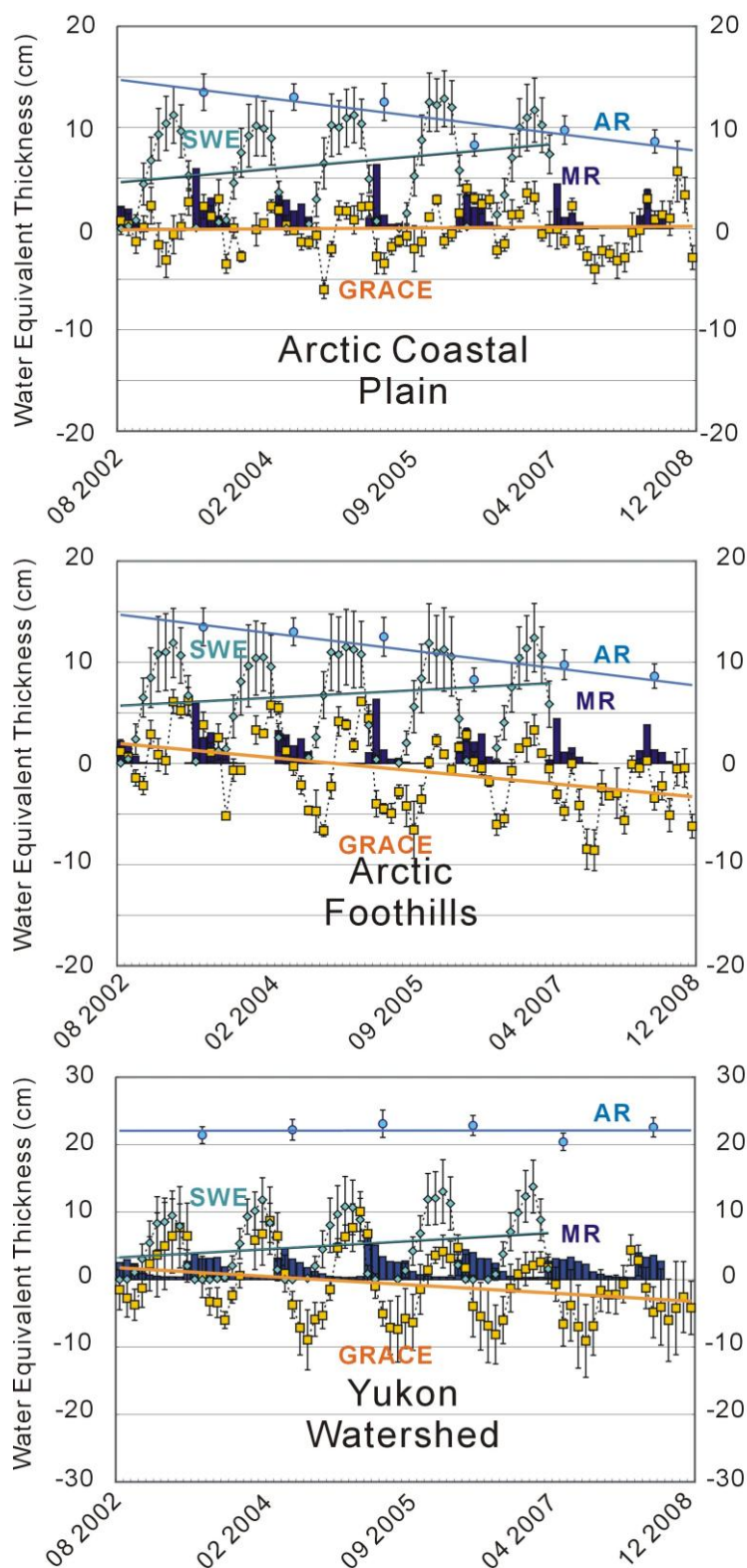
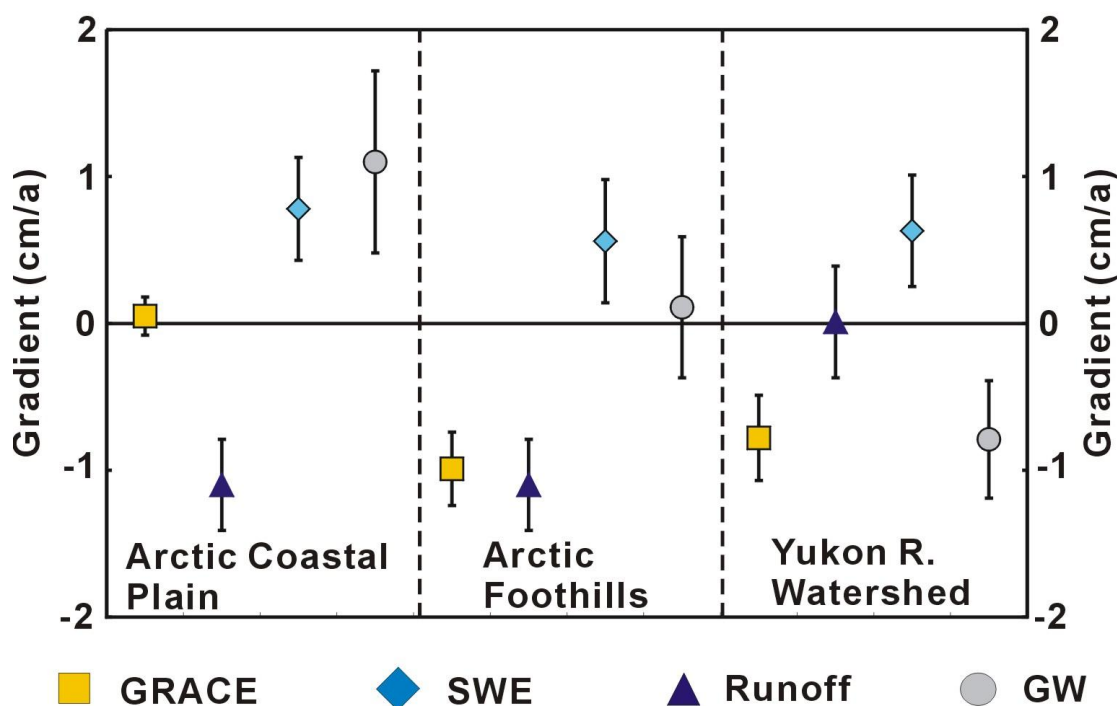


Table 1. Regionalized Gradients of GRACE (water equivalent mass), SSM/I (snow water equivalent) and Runoff Changes from August 2002 through December 2008.

A. Total Volume Change Rates			
Region	GRACE	SSM/I	Runoff
Arctic Coastal Plain	+0.06 ± 0.14 km ³ /a	+0.82 ± 0.36 km ³ /a	-1.14 ± 0.31 km ³ /a
Arctic Foothills	-0.99 ± 0.25 km ³ /a	+0.56 ± 0.42 km ³ /a	-1.14 ± 0.31 km ³ /a
Yukon Watershed	-7.37 ± 2.76 km ³ /a	+7.17 ± 3.51 km ³ /a	+0.08 ± 2.55 km ³ /a
B. Area-Average Thickness Change Rates			
Region	GRACE	SSM/I	Runoff
Arctic Coastal Plain	+0.05 ± 0.13 cm/a	+0.78 ± 0.35 cm/a	-1.10 ± 0.31 cm/a
Arctic Foothills	-0.99 ± 0.25 cm/a	+0.56 ± 0.42 cm/a	-1.10 ± 0.31 cm/a
Yukon Watershed	-0.78 ± 0.29 cm/a	+0.63 ± 0.38 cm/a	+0.01 ± 0.38 cm/a

In A. and B. runoff on the Alaskan Arctic coastal plain and foothills is integrated using the discharges from the Colville River (Umiat Station), Kuparuk River (Deadhorse), and Sagavanirktok River (Pump Station #3).

Figure 4. Regionalized gradients and uncertainties from GRACE, SSM/I and runoff, with estimated groundwater storage change: (a) volume change rates and (b) area-average thickness change. The scale on the left pertains to the Arctic coastal plain and foothills and right side pertains to the Yukon River watershed.



Runoff trends showed geographic variation north and south of the Brooks Range (Figure 4 and Table 1). The Alaska Arctic coastal plain and foothills have decreasing runoff. The Yukon River watershed shows steady (non increasing and non decreasing) runoff. The magnitudes of the uncertainty estimates, including the standard error of the trends are products of the short span of the time series.

In all cases the SSM/I trends are discordant with those from GRACE and annual runoff (Figure 4 and Table 1). The Alaskan Arctic coastal plain, foothills and the Yukon River watershed all show snow water equivalent mass gains over the period from August 2002 through December 2008.

Reduction of the GRACE total water equivalent mass change gradient by the runoff gradient yields an estimate of groundwater storage change (see section 4.1). The results indicate the Arctic coastal plain is gaining water equivalent mass (Figure 4 and Table 2). This contrasts with the Arctic foothills and the Yukon River watershed, which are losing water equivalent mass.

5.2. Geoid-Difference Model Changes

The geoid-difference model (Figure 5) shows negative geoid change gradients greatest on the large glaciers and high-elevation icefields along the mountains of central and southern Alaska and western Yukon [56-58]. Negative geoid change gradients are large on the western region of the Yukon watershed, predominately discontinuous zone, and are lesser through the remainder of the watershed, noted for relatively thin permafrost in the discontinuous and sporadic zones. Positive geoid change gradients are largest on Arctic coastal plain and the Mackenzie Delta region in the Northwest Territories, noted for their thick and ice-rich permafrost of the continuous zone and numerous thaw lake basins. The Yukon River watershed geoid change gradient is negative. The area-average geoid changes agree with the GRACE-derived regionalized groundwater storage change trends (Table 2).

Figure 5. Geoid-difference model 1-arc minute (about 2-km) grid of geoid change from 1999 through 2009.

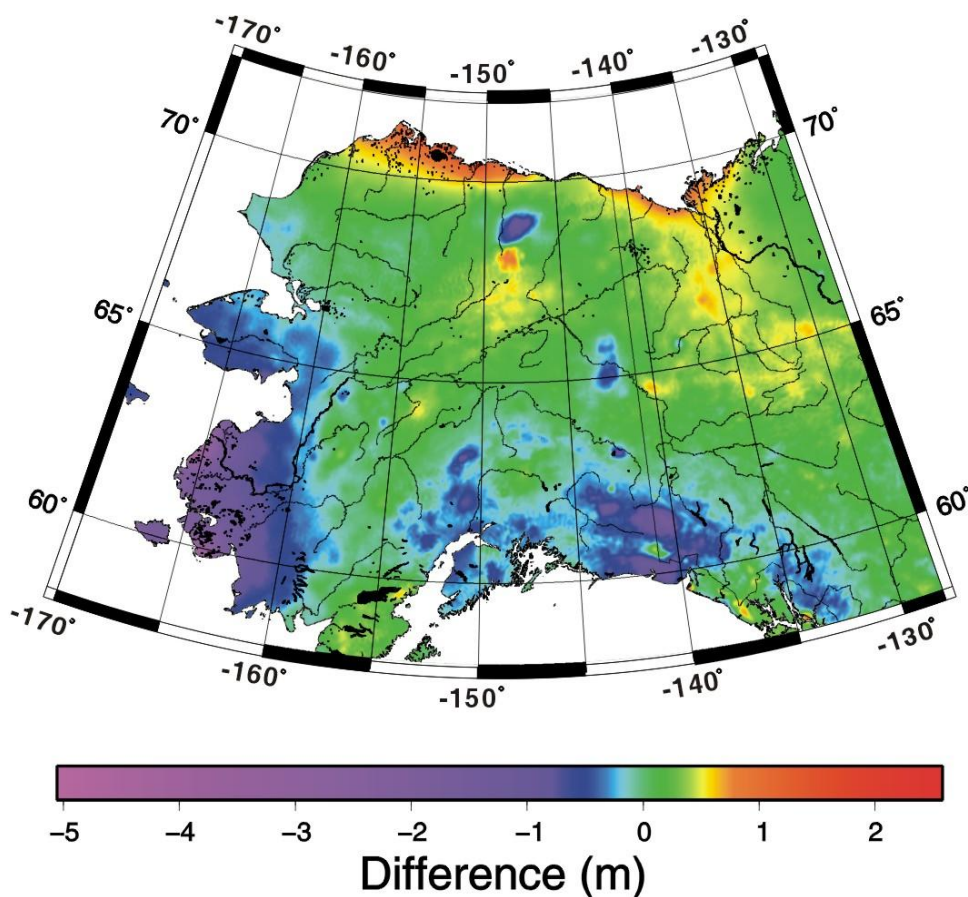


Table 2. Regionalized Groundwater Storage Gradients from GRACE and Geoid-Difference Model.

A. Total Volume Change Rates		
Region	Groundwater Storage Change	Geoid-Difference Change
Arctic Coastal Plain	+1.15 ±0.65 km ³ /a	+2.95 ±1.97 km ³ /a
Arctic Foothills	+0.11 ±0.68 km ³ /a	−0.14 ±1.37 km ³ /a
Yukon Watershed	−7.44 ±3.76 km ³ /a	−7.06 ±1.04 km ³ /a
B. Area-Average Thickness Change Rates		
Region	Groundwater Storage Change	Geoid-Difference Change
Arctic Coastal Plain	+1.10 ±0.62 cm/a	+2.83 ±1.89 cm/a
Arctic Foothills	+0.11 ±0.48 cm/a	−0.13 ±0.98 cm/a
Yukon Watershed	−0.79 ±0.40 cm/a	−0.78 ±0.11 cm/a

6. Discussions

Permafrost distribution and talik configuration affect the characteristics of surface drainage and groundwater storage changes in Arctic watersheds [5,10,11,59-61]. Watersheds with a low percentage of permafrost and well-developed talik have base flow of about 80% of discharge [10]. In watersheds with a high percentage of permafrost and poorly developed taliks, discharge can be composed of about 50% to 60% by base flow [10].

The active layer, the near-surface soil-earth layer that seasonally freezes and thaws is another factor in permafrost watersheds [59]. Changes in the active layer affect soil moisture and groundwater, ecological process and energy fluxes between the atmosphere and land [3]. Dynamics of permafrost, talik and active layer exert significant influences on surface and groundwater hydrology and geomorphology in the Arctic, and they are spatially non-uniform and nonlinear.

6.1. Alaskan Arctic Coastal Plain

The Arctic coastal plain of Alaska is a region of numerous and some quite large thermokarst thaw ponds, lakes and drained thaw lake basins [22,62]. These lakes reside in the thick ice-rich continuous permafrost zone. Their development and growth come by way of thermal processes at ice-wedge intersections and permafrost thawing with subsidence of the ground surface and increased thickness of the active layer [63]. Their elliptical shapes develop over time from thermo-erosion and wind-oriented waves that produce circulation cells. Over time, small ponds merge into large lakes, and some will drain when thermo-erosion and bank undercutting cause a breach [22,62]. Beneath the lake a talik (unfrozen soil) develops (closed talik) [59]. The talik's lateral and vertical extent depend on the internal structure of the permafrost and on the temperature regime at the ground surface. Over time talik becomes an open talik and serves as an aquifer whereby lake water drains to become subsurface groundwater (increased groundwater storage) within or in some cases below the permafrost (where it is relatively thin on the order of 10 s of meters). This indicates surface water is being recruited for subsurface groundwater storage (including ice growth) and groundwater residence time is increasing. Additional groundwater storage changes (increasing) because of increasing numbers and area of thaw bogs, ponds and lakes. Independent research indicates lakes (including thaw bogs and ponds) have been increasing in the continuous permafrost zone in Eurasia and Alaska [17,63]. On the northern

Alaskan Arctic coastal plain there is similar evidence of thaw lakes increasing, lateral spillage channels (outflow) forming on lake margins, and new pingos also appear (Guido Grosse, Personal Communication, 2009). Recent evidence also point to increased thaw penetration, which increases active layer thickness on the Arctic coastal plain of Alaska [64]. In related research we find that GRACE-derived groundwater storage is increasing in the Lena and Yenisei River watershed regions of Eurasia [18]. These watersheds encompass large areas of the continuous and discontinuous permafrost zones and talik [65].

6.2. Yukon River Watershed

An independent study of Yukon River watershed runoff indicates increasing groundwater (subsurface storage) contribution to streamflow (*i.e.*, groundwater storage loss) that currently maintains annual discharge [27]. This study pointed, in general, to permafrost thawing during the last century climate warming as having enhanced deeper flowpaths. We hypothesize that permafrost degradation is accompanied by development of taliks (which act as subsurface flowpaths) allowing intra-permafrost groundwater (either held trapped or from thawing of ice rich layers) to enter streamflow thus offsetting a negative annual net precipitation (*i.e.*, P-ET) in annual runoff. Furthermore, independent research indicates decreasing lake numbers and areas in the discontinuous permafrost zone [17,59,66]. Therefore, a component of the groundwater loss can be attributed to thaw lake shrinkage (drainage) in the Yukon River watershed of Alaska and Yukon Territory. In related research we found that GRACE-derived groundwater storage is decreasing in the Mackenzie River watershed of Canada, and groundwater storage is stable, *i.e.*, unchanged, in the Ob' River watershed of Eurasia [18]. The Mackenzie watershed is well noted for its predominately discontinuous permafrost extent and the Ob' River watershed has relative little extent of discontinuous permafrost [67].

6.3. Hypothesis

We hypothesize the changes of groundwater storage are associated with changes of surface water mass in thaw bogs, ponds, and lakes, and in subsurface water mass, possible including ice, in permafrost zones. Furthermore, we hypothesize the water mass changes are linked to changes in the character and distribution of permafrost, talik, and the active layer:

1. Increase in permafrost degradation,
2. Development of new closed- and possible open-taliks within the continuous permafrost zone,
3. Expansion of existing closed- and open-taliks and new open-taliks accompanying by decrease in volume occupied by permafrost in the discontinuous and sporadic permafrost zones,
4. Increase of taliks and active layer thickness beneath thaw lakes and rivers (increase of thaw lakes in the continuous zone and decrease of thaw lakes in the discontinuous and sporadic zones).

These physical changes in permafrost, talik and active layer serve to seasonally increase surface water storage on the Barrow Peninsula region and also to remove a portion of runoff for recruitment into subsurface groundwater storage.

Within the Yukon River watershed, the lateral reduction of permafrost, development of new open-taliks beneath thaw bog, pond, lake and river bed allows for the removal of surface water storage (thaw ponds and lakes) into groundwater storage and a portion of the groundwater storage is being recruited into runoff. Our findings agree with observations that thaw lakes have increased in the continuous permafrost zone and have decreased in the discontinuous permafrost zone [17,59,63,66].

The changes of permafrost, talik and active layer will affect groundwater residence times. On the Arctic coastal plain of Alaska groundwater residence time will increase as surface water is recruited into groundwater storage. On the Yukon River watershed groundwater residence time will decrease as groundwater leaves storage and becomes part of the river runoff (*i.e.*, discharge). This effect is in part due to the increased presence of taliks on watersheds and beneath riverbeds and serves to enhance exchange (both recruitment and export) of shallow groundwater and river water [67].

The character and changes of permafrost is strongly dependent on surface air temperature and snow cover [3,4,16]. Permafrost warming in Alaska was coincident with warming of air temperatures that began most strongly in 1976/77 in a step-like function. The Arctic coastal plain air temperatures warmed by up to 3 °C, on average, and the Yukon River watershed air temperatures warmed up by 1 °C. Surface thawing of permafrost on tundra and forest sites in Alaska was about 0.1 m/a at some locations. Basal thawing at one site was about 0.04 m/a, and accelerated to 0.09 m/a [16]. Talik provides a path for surface water to enter permafrost from above, and for groundwater to join river runoff as base flow.

On longer time scales, significant changes of permafrost and linked responses to climate and ecosystems (water cycle and carbon stocks) have occurred [6,7,10,68]. Modeling of the regional permafrost environments with general circulation model scenarios suggests significant changes in permafrost distribution are likely over the next century [69,70].

7. Conclusions

Analysis of GRACE and runoff data allow for estimates of the changes in groundwater storage. Our results indicate from 2002 through 2008:

1. Alaska Arctic coastal plain groundwater storage is increasing at $1.15 \pm 0.65 \text{ km}^3/\text{a}$ equivalent to an area-average equivalent thickness rate of $1.10 \pm 0.62 \text{ cm/a}$.
2. Yukon River watershed groundwater storage is decreasing at $7.44 \pm 3.76 \text{ km}^3/\text{a}$ equivalent to an area-average water equivalent thickness rate of $0.79 \pm 0.40 \text{ cm/a}$.

Analysis of NOAA gravimetric geoid models with isostatic glacial adjustment from continuous GPS stations indicates geoid changes from 1999 through 2009:

1. Alaska Arctic coastal plain area-average geoid change of $+2.83 \pm 1.89 \text{ cm/a}$ equivalent to $+2.95 \pm 1.97 \text{ km}^3/\text{a}$.
2. Yukon River watershed area-average geoid change of $-0.78 \pm 0.11 \text{ cm/a}$ equivalent to $-7.06 \pm 1.04 \text{ km}^3/\text{a}$.

We hypothesize these groundwater storage changes are linked to the development of new closed- and possibly open-taliks within the continuous permafrost zone associated most strongly with

the thaw ponds and lakes of the Barrow region of the Alaskan Arctic coastal plain, and expansion of existing closed and open-taliks and new open-taliks accompanied by decreasing volume occupied by permafrost in the discontinuous and sporadic permafrost zones of the Yukon River watershed in Alaska and Yukon Territory. Furthermore, our results support observations of increased bogs, ponds and lakes in the continuous permafrost zone and decreased bogs, ponds and lakes in the discontinuous permafrost zone. These changes have the potential of reducing groundwater residence-time by storage depletion (Yukon River watershed) and conversely increasing groundwater residence-time (Alaska Arctic coastal plain) by surface water recruitment into groundwater storage.

Acknowledgements

This work was funded through supporting grants from NASA (NNOG6M48G), the National Science Foundation (NSF) ARC0632400, ARC-0612533, and ARC0856864 projects, Alaska EPSCoR NSF award #EPS-0701898 and the State of Alaska. ArcticRIMS, Arctic Freshwater systems and US Geological Survey are thanked for providing hydrologic datasets. The Alaska Region Supercomputing Center and the IARC-JAXA Information System are thanked for computing facilities support. NASA and GFZ are thanked for making data available at <http://grace.jpl.nasa.gov> and http://op.gfz-potsdam.de/grace/index_GRACE.html. G. Grosse is thanked for discussion of new thaw pond, lake and pingo formation on the Arctic coastal plain of Alaska. Sergei Marchenko is thanked for helpful comments. R. Muskett performed this work at the Geophysical Institute and the International Arctic Research Center.

References and Notes

1. Rowland, J.C.; Jones, C.E.; Altmann, G.; Bryan, R.; Cosby, B.T.; Geernaert, G.L.; Hinzman, L.D.; Kane, D.L.; Lawrence, D.M.; Mancino, A.; Marsh, P.; MacNamara, J.P.; Romanovsky, V.E.; Toniolo, H.; Travis, B.J.; Trochim, E.; Wilson, C.J. Arctic landscapes in transition: Responses to thawing permafrost. *EOS Trans. AGU* **2010**, *91*, 229-236, doi:10.1029/2010EO250001.
2. Zhang, T.; Berry, R.G.; Knowles, R.G.; Heginbottom, J.A.; Brown, J. Statistics and characteristics of permafrost and ground-ice distribution in the Northern Hemisphere. *Polar Geogr.* **1999**, *23*, 132-154.
3. Romanovsky, V.E.; Osterkamp, T.E. Thawing of the active layer on the coastal plain of Alaskan Arctic. *Permafrost Periglacial Pro.* **1997**, *8*, 1-22.
4. Osterkamp, T.E.; Romanovsky, V.E. Freezing of the active layer on the coastal plain of the Alaskan Arctic. *Permafrost Periglacial Pro.* **1997**, *8*, 23-44.
5. Sergueev, D.O.; Tipenko, G.S.; Romanovsky, V.E.; Romanovskii, N.N. Evolution of mountain permafrost as a result of long-term climate change (in Russian). *Earth Cryosphere* **2003**, *7*, 15-22.
6. Romanovsky, V.E.; Sazonova, T.S.; Balohaev, V.T.; Shender, N.I.; Sergueev, D.O. Past and recent changes in air and permafrost temperatures in eastern Siberia. *Glob. Planet. Change* **2007**, *56*, 399-413, doi:10.1016/j.gloplacha.2006.07.023.

7. White, D.; Hinzman, L.; Alessa, L.; Cassano, J.; Chambers, M.; Falkner, K.; Francis, J.; Gutowski, W.J., Jr.; Holland, M.; Max Holmes, R.; Huntington, H.; Kane, D.; Kliskey, A.; Lee, C.; McClelland, J.; Peterson, B.; Rupp, T.S.; Straneo, F.; Steele, M.; Woodgate, R.; Yang, D.; Yoshikawa, K.; Zhang, T. The arctic freshwater system: Changes and impacts. *J. Geophys. Res.* **2007**, *112*, G04S54, doi:10.1029/2006JG000353.
8. Woo, M.-K. Northern hydrology. In *Canada's Cold Environments*; French, H.M., Slaymarker, O., Eds.; McGill-Queen's University Press: Montreal, QC, Canada, and Kingston, CA, USA, 1993; pp. 117-142.
9. Yoshikawa, K.; Bolton, W.R.; Romanovsky, V.E.; Fukuda, M.; Hinzman, L.D. Impacts of wildfire on the permafrost in the boreal forests of Interior Alaska. *J. Geophys. Res.* **2003**, *108*, 8148, doi:10.1029/2001JD000438.
10. Chapin, F.S., III; McGuire, D.; Ruess, R.W.; Walker, M.W.; Boone, R.D.; Edwards, M.E.; Finney, B.P.; Hinzman, L.D.; Jones, J.B.; Juday, G.P.; Kasischke, E.S.; Kielland, K.; Lloyd, A.H.; Oswood, M.W.; Ping, C.-L.; Rexstad, P.; Romanovsky, V.E.; Schimel, J.P.; Sparrow, E.B.; Sveinbjornsson, B.; Valentine, D.W.; Cleve, K.V.; Verbyla, D.L.; Viereck, L.A.; Werner, R.A.; Wurtz, T.L.; Yarie, J. Summary and synthesis: Past and future changes in the Alaskan boreal forest. In *Alaska's Changing Boreal Forest*; Chapin, F.S., III, Oswood, M.W., Cleve, K.V., Eds.; Oxford University Press Inc.: Oxford, UK, 2006; pp. 332-338.
11. Buldovich, S.; Romanovskii, N.; Tipenko, G.; Sergeev, D.; Romanovsky, V. Permafrost Dynamics within an Upper Lena River Tributary: Modeled Impact of Infiltration on the Temperature Field under a Plateau. In *Proceedings of the Ninth International Conference on Permafrost*, Fairbanks, AK, USA, 29 June–3 July 2008; pp. 211-214.
12. Romanovsky, V.E.; Osterkamp, T.E. Effects of unfrozen water on heat and mass transport processes in the active layer and permafrost. *Permafrost Periglacial Pro.* **2000**, *11*, 219-239.
13. Christiansen, H.H.; Etzelmüller, B.; Isaksen, K.; Juliussen, H.; Farbrot, H.; Humlum, O.; Johansson, M.; Ingeman-Nielsen, T.; Kristensen, L.; Hjort, J.; Holmlund, P.; Sannel, A.B.K.; Sigsgaard, C.; Åkerman, H.J.; Foged, N.; Blikra, L.H.; Pernosky, M.A.; Ødegård, R. The Thermal State of Permafrost in the Nordic area during IPY 2007–2009. *Permafrost Periglacial Pro.* **2010**, *21*, 158-181, doi:10.1002/ppp.687.
14. Romanovsky, V.E.; Drozdov, D.S.; Oberman, N.G.; Malkova, G.V.; Kholodov, A.L.; Marchenko, S.S.; Moskalenko, N.G.; Sergeev, D.O.; Ukraintseva, N.G.; Abramov, A.A.; Gilichinsky, D.A.; Vasiliev, A.A. Thermal State of Permafrost in Russia. *Permafrost Periglacial Pro.* **2010**, *21*, 136-155, doi:10.1002/ppp.683.
15. Smith, S.L.; Romanovsky, V.E.; Lewkowicz, A.G.; Burn, C.R.; Allard, M.; Clow, G.D.; Yoshikawa, K.; Throop, J. Thermal state of permafrost in North America—A contribution to the international polar year. *Permafrost Periglacial Pro.* **2010**, *21*, 117-135, doi:10.1002/ppp.690.
16. Osterkamp, T.E. Characteristics of the recent warming of permafrost in Alaska. *J. Geophys. Res.* **2007**, *112*, F02S02, doi:10.1029/2006JF000578.
17. Smith, L.C.; Sheng, Y.; MacDonald, G.M.; Hinzman, L.D. Disappearing Arctic lakes. *Science* **2005**, *308*, 1429, doi:10.1126/science.1108142.

18. Muskett, R.R.; Romanovsky, V.E. Groundwater storage changes in arctic permafrost watersheds from GRACE and *in situ* measurements. *Environ. Res. Lett.* **2009**, *4*, doi:10.1088/1748-9326/4/4/045009.
19. Osterkamp, T.E.; Payne, M.W. Estimates of permafrost thickness from well logs in northern Alaska. *Cold Reg. Sci. Technol.* **1981**, *5*, 13-27, doi:10.1016/0165-232X(81)90037-9.
20. Osterkamp, T.E.; Gosink, J.P. Variations in permafrost thickness in response to changes in paleoclimate. *J. Geophys. Res.* **1991**, *96*, 4423-4434.
21. Jorgenson, T.; Yoshikawa, K.; Kanevskiy, M.; Shur, Y.; Romanovsky, V.; Marchenko, S.; Grosse, G.; Brown, J.; Jones, B. *Permafrost Characteristics of Alaska (Map, Updated)*; Institute of Northern Engineering, University of Alaska: Fairbanks, AK, USA, 2008.
22. Hinkel, K.M.; Frohn, R.C.; Nelson, F.E.; Eisner, W.R.; Beck, R.A. Morphometric spatial analysis of thaw lakes and drained thaw lake basins in the western Arctic coastal plain, Alaska. *Permafrost Periglacial Pro.* **2005**, *16*, 327-341, doi:10.1002/ppp.532.
23. Molnia, B.F. Glaciers of North America—Glaciers of Alaska. In *Satellite Image Atlas of the Glaciers of the World*, Williams, R.S., Jr., Ferrigno, J.G., Eds.; US Geological Survey Prof. Paper 1386-K; US Department of Interior, US Government Printing Office: Washington, DC, USA, 2008.
24. Shulski, M.; Wendler, G. *The Climate of Alaska*; University of Alaska Press: Fairbanks, AK, USA, 2007.
25. Sturm, M.; Liston, G.E. The snow cover on lakes of the Arctic coastal plain of Alaska, USA. *J. Glaciol.* **2003**, *49*, 370-380, doi:10.3189/1727565033781830539.
26. Atwood, D.K.; Guritz, R.M.; Muskett, R.R.; Lingle, C.S.; Sauber, J.M.; Freymueller, J.T. DEM control in Arctic Alaska with ICESat laser altimetry. *IEEE Trans. Geosci. Remote Sens.* **2007**, *45*, 3710-3720, doi:10.1109/TGRS.2007.904335.
27. Walvoord, M.A.; Striegl, R.G. Increased groundwater to stream discharge from permafrost thawing in the Yukon River basin: Potential impacts on lateral export of carbon and nitrogen. *Geophys. Res. Lett.* **2005**, *34*, L12402, doi:10.1029/2007GL030216.
28. Brabets, T.P.; Wang, B.; Meade, R.H. *Environmental and Hydrologic Overview of the Yukon River Basin, Alaska and Canada*; Water-Resources Investigations Report 99-4204; US Geological Survey: Anchorage, AK, USA, 2000.
29. Yang, D.; Zhao, Y.; Armstrong, R.; Robinson, D. Yukon River streamflow response to seasonal snow cover changes. *Hydrol. Process.* **2009**, *23*, 109-121, doi:10.1002/hyp.7216.
30. Striegl, R.G.; Aiken, G.R.; Dornblaser, M.M.; Raymond, P.A.; Wickland, K.P. A decrease in discharge-normalized DOC export by the Yukon River during summer through autumn. *Geophys. Res. Lett.* **2005**, *32*, L21413, doi:10.1029/2005GL024413.
31. Woodgate, R.A.; Aagaard, K. Revising the Bering Strait freshwater flux into the Arctic Ocean. *Geophys. Res. Lett.* **2005**, *32*, L02602, doi:10.1029/2004GL021747.
32. Smith, D.A.; Milbert, D.G. The GEOID96 high-resolution geoid height model for the United States. *J. Geod.* **1999**, *73*, 219-236.
33. Smith, D.A.; Roman, D.R.: GEOID99 and G99SSS: 1-arc-minute geoid models for the United States. *J. Geod.* **2001**, *75*, 469-490.

34. Lemoine, F.G.; Kenyon, S.C.; Factor, J.K.; Trimmer, R.G.; Palvis, N.K.; Chinn, D.S.; Cox, C.M.; Klosko, S.M.; Luthcke, S.B.; Torrence, M.H.; Wang, Y.M.; Williamson, R.G.; Pavlis, E.C.; Rapp, R.H.; Olson, T.R. *The Development of the Joint NASA GSFC and the National Imagery and Mapping Agency (NIMA) Geopotential Model EGM96*; NASA/TP-1998-206861; NASA Goddard Space Flight Center: Greenbelt, MD, USA, 1998.
35. Altamimi, Z.; Collilieux, X.; Legrand, J.; Garayt, B.; Boucher, C. ITRF2005: A new release of the International Terrestrial Reference Frame on time series of station positions and Earth orientation parameters. *J. Geophys. Res.* **2007**, *112*, B09401, doi:10.1029/2007JB004949.
36. Sandwell, D.T. Biharmonic spline interpolation of GOES-3 and SEASAT altimeter data. *Geophys. Res. Lett.* **1987**, *14*, 139-142.
37. Wessel, P. A general-purpose Green's function-based interpolator. *Comput. Geosci.* **2009**, *35*, 1247-1254, doi:10.1016/j.cageo.2008.08.012.
38. Wahr, J.; Molenaar, M.; Bryan, F. Time variability of the Earth's gravity field: Hydrologic and oceanic effects and their possible detection using GRACE. *J. Geophys. Res.* **1998**, *103*, 30205-30229, doi:10.1029/98JB02844.
39. Tapley, B.D.; Bettadpur, S.; Ries, J.C.; Thompson, P.F.; Watkins, M.M. GRACE measurements of mass variability in the Earth system. *Science* **2004**, *305*, 503-505, doi:10.1126/Science.1099192.
40. Tapley, B.D.; Bettadpur, S.; Watkins, M.; Reigber, C. The gravity recovery and climate experiment: Mission overview and early results. *Geophys. Res. Lett.* **2004**, *31*, L09607, doi:10.1029/2004GL019920.
41. Quinn, K.J.; Ponte, R.M. Uncertainty in ocean mass trends from GRACE. *Geophys. J. Int.* **2010**, *181*, 762-768, doi:10.1111/j.1365-426X.201004508.x.
42. Zenner, L.; Gruber, T.; Jäggi, A.; Beutler, G. Propagation of atmospheric model errors to gravity potential harmonics—Impact on GRACE de-aliasing. *Geophys. J. Int.* **2010**, *182*, 797-807, doi:10.1111/j.1365-246X.2010.04669.
43. Peltier, W.R. Global glacial isostasy and the surface of the Ice-Age Earth: The ICE-5G (VM2) model and GRACE. *Ann. Rev. Earth Planet. Sci.* **2004**, *32*, 111-149, doi:10.1146/annurev.earth.32.082503.144359.
44. Paulson, A.; Zhong, S.; Wahr, J. Inference of mantle viscosity from GRACE and relative sea level data. *Geophys. J. Int.* **2007**, *171*, 497-508, doi:10.1111/j.1365.246X.2007.03556.x.
45. Armstrong, R.L.; Brodzik, M.J.; Knowles, K.; Savie, M. *Global Monthly EASE-Grid Snow Water Equivalent Climatology*; Digital Media B; National Snow and Ice Data Center: Boulder, CO, USA, 2007.
46. Chang, A.T.C.; Foster, J.L.; Hall, D.K. Nimbus-7 SMMR derived global snow cover parameters. *Ann. Glaciol.* **1987**, *9*, 39-44.
47. Armstrong, R.L.; Brodzik, M.J. Recent northern hemisphere snow extent: A comparison of data derived from visible and microwave sensors. *Geophys. Res. Lett.* **2001**, *28*, 3673-3676.
48. Chang, A.T.C.; Foster, J.L.; Kelly, R.E.J.; Josberger, E.G.; Armstrong, R.L.; Mognard, N.M. Analysis of ground-measured and passive-microwave-derived snow depth variations in midwinter across the northern Great Plains. *J. Hydromet.* **2005**, *6*, 20-33, doi:10.1175/jhm-404.1.

49. Shiklomanov, A.I.; Yakovleva, T.I.; Lammers, R.B.; Karasev, I.Ph.; Vorosmarty, C.J.; Linder, E. Cold region river discharge uncertainty—Estimates from large Russian rivers. *J. Hydrol.* **2006**, *326*, 231-256, doi:10.1016/j.hydrol.2005.10.037.
50. Wahl, K.L.; Thomas, W.O., Jr.; Hirsch, R.M. *Stream-Gauge Program of the US Geologic Survey*; US Geologic Survey Circular 1123; USGS: Reston, VA, USA, 1995.
51. Güntner, A. Improvement of global hydrologic models using GRACE data. *Surv. Geophys.* **2008**, *29*, 375-397, doi:10.1007/s.100712-008-9038-y.
52. Kuche, J.; Schmidt, R.; Petrovic, S.; Rietbroek, R. Decorrelated GRACE time-variable gravity solutions from GFZ, and their validation using a hydrological model. *J. Geod.* **2009**, *83*, 903-913, doi:10.1007/s00190-009-0308-3.
53. Bevington, P.R.; Robinson, D.K. *Data Reduction and Error Analysis for the Physical Sciences*, 2nd ed.; McGraw-Hill, Inc.: New York, NY, USA, 1992.
54. Levitan, B.M. Hilbert space. In *Encyclopaedia of Mathematics*; Hazewinkel, M., Ed.; Springer-Verlag: Berlin, Germany, 2002. Available online: <http://eom.springer.de/H/h047380.htm> (accessed on 22 February 2011).
55. Blakely, R.J. *Potential Theory in Gravity and Magnetic Applications*; Cambridge University Press: Cambridge, UK, 1996.
56. Muskett, R.R.; Lingle, C.S.; Sauber, J.M.; Rabus, B.T.; Tangborn, W.V. Acceleration of surface lowering on the tidewater glaciers of Icy Bay, Alaska, USA from InSAR DEMs and ICESat altimetry. *Earth Planet. Sci. Lett.* **2008**, *265*, 345-359, doi:10.1016/j.epsl.2007.10.012.
57. Muskett, R.R.; Lingle, C.S.; Sauber, J.M.; Post, A.S.; Tangborn, W.V.; Rabus, B.T. Surging, accelerating surface lowering and volume reduction of the Malaspina Glacier system, Alaska, USA, and Yukon, Canada from 1972 to 2006. *J. Glaciol.* **2008**, *54*, 788-800.
58. Muskett, R.R.; Lingle, C.S.; Sauber, J.M.; Post, A.S.; Tangborn, W.V.; Rabus, B.T.; Echelmeyer, K.A. Airborne and spaceborne DEM- and laser altimetry-derived surface elevation and volume changes of the Bering Glacier system, Alaska, USA, and Yukon, Canada, 1972–2006. *J. Glaciol.* **2009**, *55*, 316-326.
59. Yoshikawa, K.; Hinzman, L.D. Shrinking thermokarst ponds and groundwater dynamics in discontinuous permafrost near council, Alaska. *Permafrost Periglacial Pro.* **2003**, *14*, 151-160.
60. Yoshikawa, K.; Romanovsky, V.; Hinzman, L.; Zheleznyak, M.; Romanovskii, N.; Buldovich, S. Intra-permafrost water and hydrological chronology: A case study of aufeis and spring hydrology in continuous permafrost regions. *EOS Trans. AGU Fall Meeting Suppl.* **2006**, Abstract U31B-07.
61. Oberman, N. Contemporary Permafrost Degradation of European North of Russia. In *Proceedings Ninth International Conference on Permafrost*, Fairbanks, AK, USA, 29 June–3 July 2008; Volume 2, pp. 1305-1310.
62. Hinkel, K.M.; Eisner, W.R.; Bockheim, J.G.; Nelson, F.E.; Peterson, K.M.; Dai, X. Spatial extent, age, and carbon stocks in drained thaw lakes basins on the Barrow Peninsula, Alaska. *Arc. Ant. Alpine Res.* **2003**, *35*, 291-300.
63. Jorgenson, M.T.; Shur, Y.L.; Pullman, E.P. Abrupt increase in permafrost degradation in Arctic Alaska. *Geophys. Res. Lett.* **2006**, *33*, L02503, doi:10.1029/2005GL024960.

64. Pullman, E.R.; Jorgenson, M.T.; Shur, Y. Thaw settlement in soils of the Arctic coastal plain Alaska. *Arc. Ant. Alpine Res.* **2007**, *39*, 468-476.
65. Serreze, M.C.; Bromwich, D.H.; Clark, M.P.; Etringer, A.J.; Zhang, T.; Lammers, R. Large-scale hydor-climatology of the terrestrial Arctic drainage system. *J. Geophys. Res.* **2003**, *108*, D2, 8160, doi:10.1029/2001JD000919.
66. Riordan, B.; Verbyla, D.; McGuire, A.D. Shrinking ponds in subarctic Alaska based on 1950–2002 remotely sensed images. *J. Geophys. Res.* **2006**, *111*, G04002, doi:10.1029/2005JG000150.
67. Zarnetske, J.P.; Gooseff, M.N.; Bowden, W.B.; Greenwald, M.J.; Brosten, T.R.; Bradford, J.H.; McNamara, J.P. Influence of morphology and permafrost dynamics on hyporheic exchange in Arctic headwater streams under warming climate conditions. *Geophys. Res. Lett.* **2008**, *35*, L02501, doi:10.1029/2007GL032049.
68. Ping, C.L.; Michaelson, J.; Jorgenson, M.T.; Kimble, J.M.; Epstein, H.; Romanovsky, V.E.; Walker, D.A. High stocks of soil organic carbon in the North American Arctic region. *Nature Geosci.* **2008**, *1*, 615-619, doi:10.1038/ngeo284.
69. Sazonova, T.S.; Romanovsky, V.E.; Walsh, J.E.; Sergueev, D.O. Permafrost dynamics in the 20th and 21st centuries along the east Siberian transect. *J. Geophys. Res.* **2004**, *109*, D01108, doi:10.1029/2003JD003680.
70. Shuur, E.A.G.; Bockheim, J.; Canadell, J.G.; Euskirchen, E.; Field, C.B.; Goryachkin, S.V.; Hagemann, S.; Kury, P.; Lafleur, P.M.; Lee, H.; Mazhitova, G.; Nelson, F.E.; Rinke, A.; Romanovsky, V.E.; Shiklomanov, N.; Tarnocai, C.; Venevsky, S.; Vogel, J.G.; Zimov, S.A. Vulnerability of permafrost carbon to climate change: Implications for global carbon cycle. *BioScience* **2008**, *58*, 701-714, doi:10.1641/B580807.

© 2011 by the authors; licensee MDPI, Basel, Switzerland. This article is an open access article distributed under the terms and conditions of the Creative Commons Attribution license (<http://creativecommons.org/licenses/by/3.0/>).